Does surface roughness necessarily increase fouling propensity of polyamide reverse osmosis membranes by humic acid?

Qimao Gan,[†] Chenyue Wu,[†] Li Long,[†] Lu Elfa Peng,[*,†] Zhe Yang,[†] Hao Guo,[†] Chuyang Y. Tang[*,†]

[†]Department of Civil Engineering, The University of Hong Kong, Pokfulam, Hong Kong SAR 999077, P. R. China.

[*]Corresponding Authors:

Lu Elfa Peng, Email: elfapeng@connect.hku.hk, Phone: +852-53964327

Chuyang Y. Tang, Email: tangc@hku.hk, Phone: +852-28591976

20 **TABLE OF CONTENT**

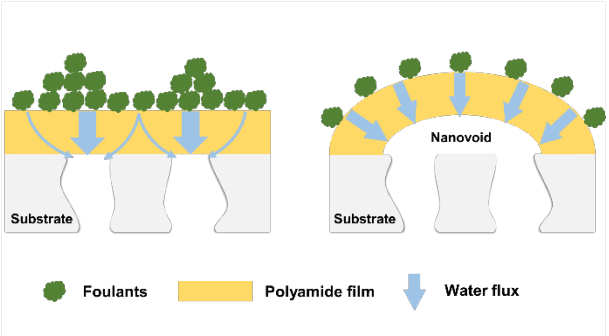

21

22

ABSTRACT

Surface roughness has crucial influence on fouling propensity of thin film composite (TFC) polyamide reverse osmosis (RO) membranes. A common wisdom is that rougher membranes tend to experience more severe fouling. In this study, we compared the fouling behaviors of a smooth polyamide membrane (RO-s) and a nanovoid-containing rough polyamide membrane (RO-r). In contrary to the traditional belief, we observed more severe fouling for RO-s, which can be ascribed to its uneven flux distribution caused by the 'funnel effect'. Additional tracer filtration tests using gold nanoparticles revealed a more patch-like particle deposition pattern, confirming the adverse impact of 'funnel effect' on membrane water transport. In contrast, the experimentally observed lower fouling propensity of the nanovoid-containing rough membrane can be explained by: (1) the weakened 'funnel effect' thanks to the presence of nanovoids, which can regulate the water transport pathway through the membrane; and (2) the decreased average localized flux over the membrane surface due to the increased effective filtration area for the nanovoid-induced roughness features. The current study provides fundamental insights into the critical role of surface roughness in membrane fouling, which may have important implications to the future development of high-performance antifouling membranes.

KEYWORDS: *polyamide reverse osmosis (RO) membranes, surface roughness, membrane fouling, funnel effect, nanovoid-containing roughness structure*

SYNOPSIS: Nanovoids contained in a rough polyamide RO membrane reduce the fouling propensity by simultaneously improving the water transport pathway through the membrane and increasing the effective filtration area.

INTRODUCTION

Water scarcity has become an urgent concern because of population boom, rapid industrialization, and severe water pollution at a global scale.[1, 2] Alternative water supply through membrane-based desalination and water reuse using reverse osmosis (RO) has played a vital role in addressing this concern.[2-6] However, the separation performance of RO membranes is severely affected by fouling, thereby compromising the process efficiency and quality of product water.[6-9] To facilitate the development of effective antifouling strategies, mechanistic understanding of membrane fouling is of great necessity.[1, 10]

Among the various factors influencing membrane fouling,[7, 9, 11-13] membrane surface roughness is considered as a crucial factor.[7, 10, 11, 14] A common wisdom is that a rougher membrane surface tends to suffer more severe fouling. For example, Elimelech and coworkers observed faster fouling rate for fully aromatic polyamide membranes compared to semi-aromatic polyamide membranes[15, 16] and cellulose acetate membranes[17], which was attributed to the 'ridge-and-valley' roughness structure of the former. However, these studies involved different membrane chemistry (e.g., smooth cellulose acetate membrane vs. rough polyamide membrane[17]), which may affect the membrane-foulant interactions and thus the fouling tendency.[7, 18] Several other studies reported a similar trend,[13, 19, 20] citing preferential accumulation of foulants in the 'valleys' as a key reason for accelerated fouling. In contrast, several recent studies[21-23] reported the use of micro-patterned surfaces (e.g., biomimetic sharklet[21] and line-and-space gratings[22]) for mitigating fouling propensity by surface pattern-induced hydrodynamic flows (e.g., eddies), despite that such micropatterns would contribute to greater membrane surface roughness. At a nanometer

scale, roughness features in the form of nanostripes,[24] nanocapsules,[25] and belt-crater morphology[26, 27] were also found to reduce fouling propensity. These contradictory results in existing literature prompt us to revisit the fundamental role of surface roughness in membrane fouling.

In-depth understanding of water transport through polyamide rejection layers could potentially provide an alternative angle to interpret membrane fouling behavior. Water transport through a thin film composite (TFC) polyamide membrane could be severely constrained by the 'funnel effect' due to the limited porosity of the substrate (Figure 1a):[28-31] (1) the part of polyamide directly above substrate pores can efficiently conduct water to reach the pores, but (2) that away from the pores are far less efficient in water transport due to the much longer path length to reach the pores.[30-34] Since the first report of the "funnel effect" by Lonsdale et al.[28] in 1971, several other groups further investigated this phenomenon.[29-31, 35, 36] Of particular interest, a few modeling studies[34, 37-39] show that the 'funnel effect' could create highly uneven flux distribution with localized hot spots of high flux above the substrate pores and suggest that this phenomenon could have major implications for membrane fouling. Since fouling is greatly influenced by the localized water flux,[34, 38, 39] a severe 'funnel effect' is expected to result in greater fouling.[31]

Recent literature shows that the 'ridge-and-valley' roughness structure in TFC RO membranes is caused by nanovoids encapsulated in the polyamide layer.[40-43] These nanovoids were found to be well correlated to membrane water permeance.[39, 44-47] Presumably, the presence of nanovoids can modify the water transport pathway through the membrane.[34, 38, 39, 44] Since the nanovoids connect well to the substrate pores,[41, 45, 46] water can now transport through the polyamide film in the normal direction with the least

hydraulic resistance (Figure 1b). Thus, a rougher TFC membrane could potentially weaken the 'funnel effect' and improve the flux distribution, which would mitigate membrane fouling. Moreover, a rougher membrane surface provides greater effective filtration area for water transport (Figure 1b),[48-50] which can decrease the average localized flux over the membrane surface (i.e., total flow normalized by the effective filtration area) under a given apparent flux (i.e., total flow normalized by the membrane plan area). These potential beneficial effects of nanovoids prompt us to hypothesize that a nanovoid-containing rough polyamide membrane could be more fouling resistant compared to a smooth polyamide membrane.

To reveal the effect of surface roughness (and nanovoids) on membrane fouling, we prepared a rough and a smooth polyamide membrane with an identical recipe for interfacial polymerization (IP), except that the smooth membrane was prepared at a free interface to eliminate the formation of nanovoids.[42, 43] We demonstrate a significantly reduced fouling tendency of the rougher membrane using humic acid (HA), which was further confirmed by additional tracer filtration tests using gold nanoparticles. In a word, this study provides an alternative angle and fundamental mechanisms to re-think the critical role of surface roughness on membrane fouling. Our findings have major implications to the future development of high-performance antifouling membranes, particularly with respect to the design of membrane morphology.

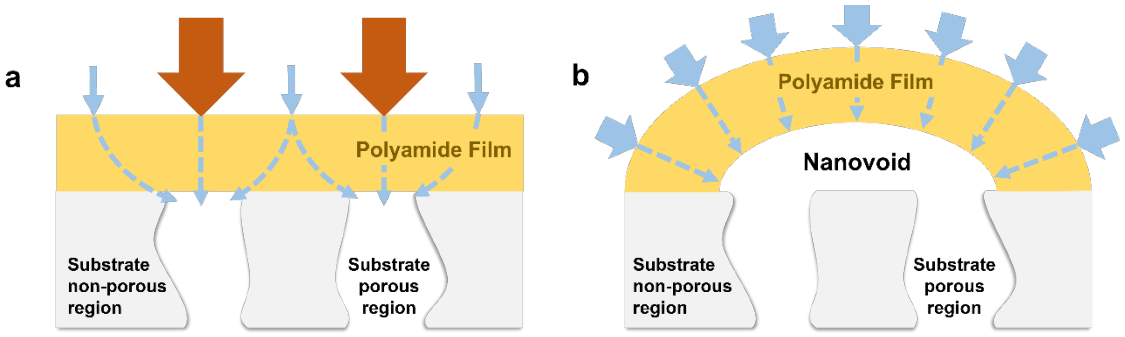

Figure 1. Water transport pathway through (a) smooth polyamide film with uneven water distribution ('funnel effect'), and through (b) rough polyamide film containing nanovoids with modified water transport pathway and larger effective filtration area.

MATERIALS AND METHODS

Chemicals. A commercial polysulfone (PSf) ultrafiltration membrane (molecular weight cutoff 67 kDa, Vontron Technology) was used as the substrate for both the rough and smooth polyamide RO membranes. *m*-phenylenediamine (MPD, 99%), trimesoyl chloride (TMC, 98%), and *n*-hexane obtained from Sigma-Aldrich were used in the IP reaction to prepare polyamide RO membranes. Sodium chloride (NaCl, Dieckmann) was used for separation performance tests. Humic acid (HA, Sigma-Aldrich) and calcium chloride ($CaCl_2$, Dieckmann) were used for fouling tests. Hydrochloric acid (HCl, Dieckmann) was used to adjust the pH of feed solution. Sodium hydroxide (NaOH, Dieckmann) was used to extract the accumulated HA on fouled membranes. Dimethyformamide (DMF, Dieckmann) was used to dissolve PSf substrate for observing the backside of polyamide layer (see the Supporting Information S1).

Preparation of rough polyamide RO membranes. The rough polyamide RO membranes were prepared using a traditional IP process on PSf substrates. Typically, a PSf substrate was first immersed in a 2 w/w% MPD solution for 2 min. After removing the excess MPD solution by a rubber roller, the substrate was soaked in a 0.1 w/w% TMC/hexane solution for 1 min to form the polyamide layer. The resulted polyamide membrane was rinsed with hexane and further post-treated in 50 °C Milli-Q water for 10 min. The prepared rough polyamide RO membranes were named as RO-r.

Preparation of smooth polyamide RO membranes. The relatively smooth polyamide RO membranes were prepared under free-interface IP process.[42, 43] Briefly, a 0.1 w/w% TMC/hexane solution was gently added onto a 2 w/w% MPD solution to react for 1 min. The resultant polyamide layer was then loaded onto the PSf substrate by vacuum filtration.

After removing the excess TMC solution, the membrane was cleaned by hexane. The prepared polyamide RO membranes were named as RO-s.

Membrane characterization. Field-emission scanning electron microscopy (FE-SEM, S-4800, Hitachi) at an accelerating voltage of 5 kV was used to characterize the surface structure of membranes. Before SEM characterization, all the membrane samples were first dried at 40 ℃ in an oven, and then sputter coated by gold for 40 s. In addition to the top-side surface, the backside of the polyamide layer was also examined by SEM after dissolving PSf using DMF (see the Supporting Information S1).[41, 42]

The membrane cross-sectional images were characterized using transmission electron microscopy (TEM, CM100, Philips) at an accelerating voltage of 100 kV. All the membrane samples were soaked in 10 v/v% glycerol/water for 1 h and dried before TEM characterization.[42, 43] The membrane surface roughness was measured by atomic force microscopy (AFM) with a scanning area of $5\times5\ \mu m^2$. The membrane surface charge property was characterized by a streaming potential analyzer (SurPASS, Anton Paar, Austria). The membrane water contact angle was obtained using an automatic contact angle meter (Attension Theta, Biolin Scientific, Sweden) equipped with a video capture device. The ionized carboxyl group density of polyamide layer was quantified at different pHs using silver ion bind-and-elute method (see the Supporting Information S2).[51, 52]

Membrane separation performance. The separation performances were tested using a laboratory-scale crossflow RO filtration system.[53] A membrane sample with a plan area of 12 cm^2 was applied in a stainless-steel cell. After pre-compacted at 17.0 bar for 1.5 h using 2000 ppm NaCl feed solution at a crossflow velocity of 22.4 cm/s under room temperature (~25 °C), the permeate samples were collected at 15.5 bar and their water flux and salt

rejection were measured. The water flux J_v (L m^{-2} h^{-1}) and water permeance A (L m^{-2} h^{-1} bar^{-1}) were calculated by:

$$J_v = \frac{\Delta m}{\Delta t \times a \times \rho} \quad (1)$$

$$A = \frac{J_v}{\Delta P - \Delta \pi} \quad (2)$$

where Δm (kg) is the mass of permeate over a time interval of Δt (h), a (m^2) is the membrane filtration area (plan area), ρ is the density of water, ΔP (bar) is the applied pressure, and $\Delta \pi$ (bar) is the transmembrane osmotic pressure.

The salt rejection R was calculated based on the conductivity of the feed solution (C_f) and that of the permeate (C_p) measured by a portable conductivity meter (Ultrameter II, Myron L):

$$R = \frac{C_f - C_p}{C_f} \times 100\% \quad (3)$$

Membrane fouling tests. A membrane sample with a plan area of 12 cm^2 was applied in a stainless-steel cell and was pre-compacted with a 2000 ppm NaCl feed solution at 17.0 bar for 12 h at a crossflow velocity of 11.2 cm/s under room temperature (~25 °C). To conduct the fouling test, the initial flux (J_0) was adjusted to 15 or 20 L m^{-2} h^{-1} and maintained stable for 0.5 h. A 100 ppm HA was then added into the feed solution to start membrane fouling. Fouling tests were also performed under pH of 4.0 to exclude the effect of ionized carboxyl groups on fouling propensity. In addition, the effect of calcium was evaluated by conducting fouling tests with 0 or 0.1 mM $CaCl_2$ in the feed solution. Each fouling test was continued for 48 h, and the permeate flux measured at 48 h was denoted as J_1.

The fouled membranes were cleaned with DI water at a crossflow velocity of 22.4 cm/s for 0.5 h under no applied pressure. After this cleaning step, the same pressure was applied again to measure the membrane permeate flux using the 2000 ppm NaCl solution (J_2). The irreversible flux reduction (R_{ir}),[31] reversible flux reduction (R_r),[31] and flux recovery efficiency (E_r)[54] were evaluated by:

$$R_{ir} = \frac{J_0 - J_2}{J_0} \times 100\% \quad (4)$$

$$R_r = \frac{J_2 - J_1}{J_0} \times 100\% \quad (5)$$

$$E_r = \frac{J_2 - J_1}{J_0 - J_1} \times 100\% \quad (6)$$

Gold nanoparticle filtration tests. The gold nanoparticle filtration tests (1.0×10^{12} particles/mL) were performed using a dead-end filtration setup under an identical flux of 6 L m^{-2} h^{-1} for 2 h at the temperature of 25 °C. To obtain the TEM plan view, DMF was used to dissolve the membrane substrates before the polyamide film was loaded onto a TEM grid. Then, the samples were dried at 60 °C for 10 min before the characterization.

RESULTS AND DISCUSSION

Membrane surface properties and separation performance of RO-s and RO-r.

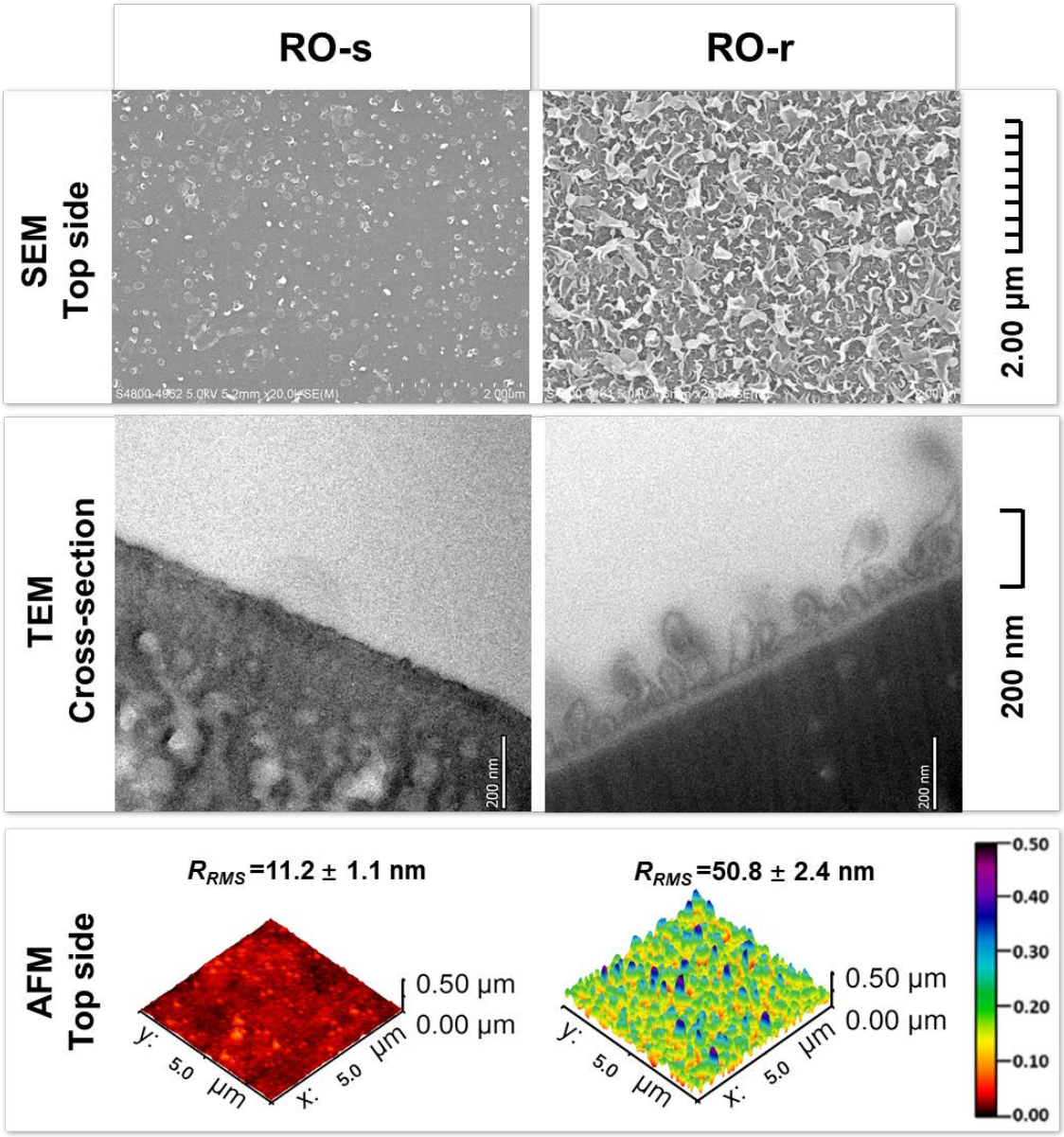

Figure 2. Surface properties of RO-s and RO-r membranes including surface roughness micrographs of SEM (top sides), TEM (cross-sections), and AFM (top sides).

As expected, RO-s gave a smooth surface with some small nodules (SEM micrograph, left column in Figure 2) and negligible nanovoids (TEM micrograph, left column in Figure 2),

accompanied by a low roughness of 11.2 nm (AFM micrograph, left column in Figure 2) and surface area ratio of 1.16 (Table 1). In contrast, RO-r presented a typical 'ridge-and-valley' surface structure (SEM micrograph, right column in Figure 2) containing numerous nanovoids (TEM micrograph, right column in Figure 2) with a high roughness of 50.8 nm (AFM micrograph, right column in Figure 2) and surface area ratio of 2.98 (Table 1). The different surface morphology of the two membranes can be explained by nanobubble formation during the IP reaction.[40, 41, 43] Retention of these nanobubbles between the polyamide layer and the substrate results in nanovoids-containing rough structures (i.e., for RO-r).[40-42] In the absence of substrate, the nanobubbles could escape from the substrate-free interface, forming a smooth polyamide film (i.e., for RO-s).[42, 43, 55]

Accordingly, the backside polyamide layer of RO-r exhibited a honeycomb-like structure with numerous openings in contrast to the negligible openings on RO-s (Figure 3). According to previous studies, these openings connect the nanovoids to the substate pores,[41, 45, 46] and they are possibly caused by the escape of gas/vapor from the IP reaction interface to the porous substrate.[42] Furthermore, RO-r presented higher water permeance with similar NaCl rejection compared with RO-s (97.7 ± 0.3% for RO-r vs. 97.4 ± 0.5% for RO-s, Figure 4a). The high permeance of RO-r can be well correlated with its prominent nanovoids and openings. As depicted in Figure 1b, these voids not only shorten the water transport pathway through the polyamide film of membrane[34, 38, 39, 44] but also increase the effective filtration area.[48-50] Moreover, more openings at the backside polyamide layer of RO-r can improve the connectivity between the nanovoids and substate pores, which can benefit the efficient water collection into the pores.[41, 46, 56] In respect to other surface

properties, RO-r has a similar water contact angle to RO-s (p = 0.0523, Figure 4b) and is slightly less negatively charged than RO-s (Figure 4c).

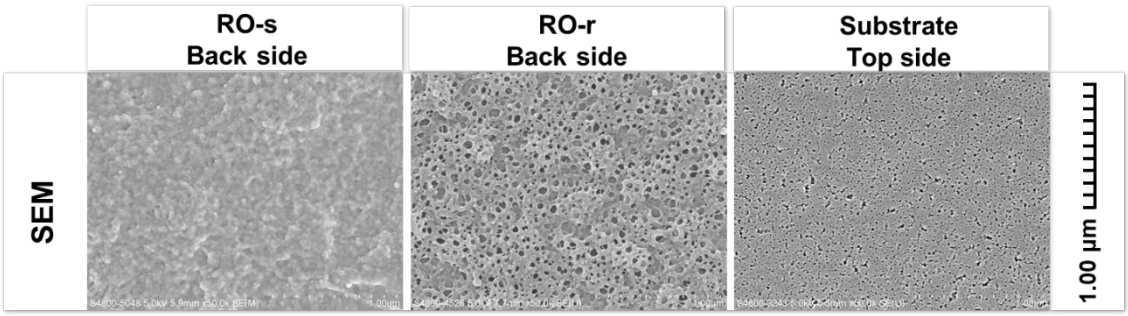

Figure 3. SEM micrographs on the backside polyamide layer of RO-s and RO-r and topside of the substrate.

Table 1. Properties of polyamide layer and substrate

Sample	RO-s	RO-r	Substrate
Surface roughness (R_{RMS}, nm)	11.2 ± 1.1	50.8 ± 2.4	-
Surface area ratio	1.16 ± 0.01	2.98 ± 0.16	-
Opening/pore number density (counts/µm^2)	-	148 ± 8	507 ± 37
Opening/pore area coverage (%)	-	32.5 ± 0.9	16.5 ± 0.8
Opening/pore average diameter (nm)	-	52.9 ± 11.3	20.3 ± 3.2

The number density, area coverage, and average diameter of polyamide layer backside openings and substrate pores, and surface area ratio of polyamide layer topside were characterized based on the SEM and TEM micrographs using the software *Image pro plus*.

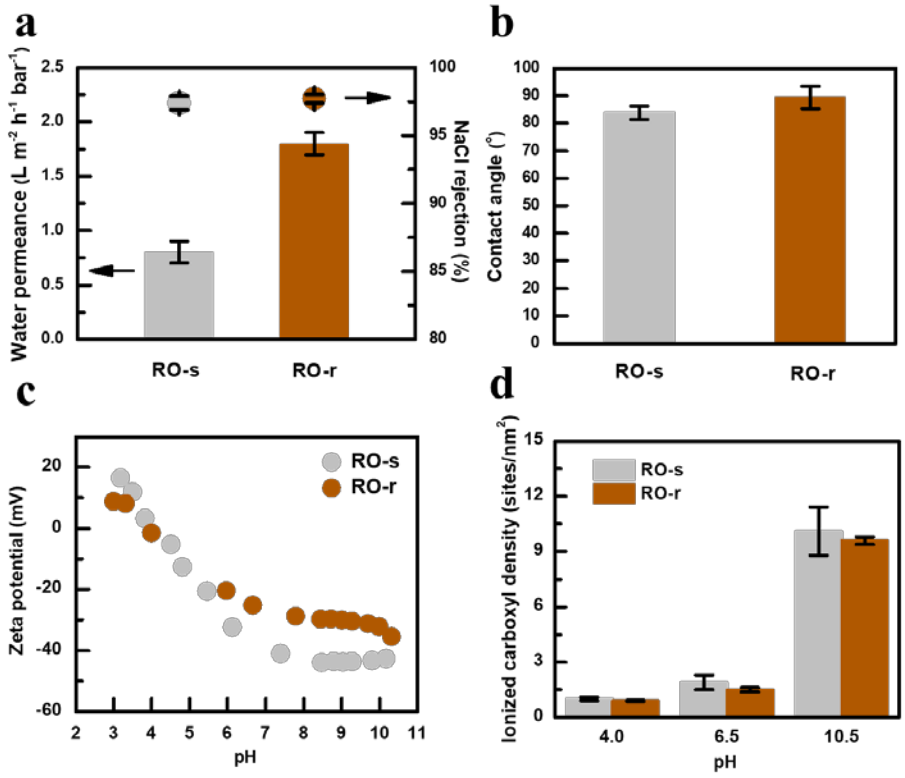

232

233 Figure 4. (a) Separation performance, (b) water contact angle, (c) Zeta potential, and (d) ionized carboxyl
234 group density at different pHs of RO-s and RO-r.

235

236

Water transport pathway of RO-s and RO-r

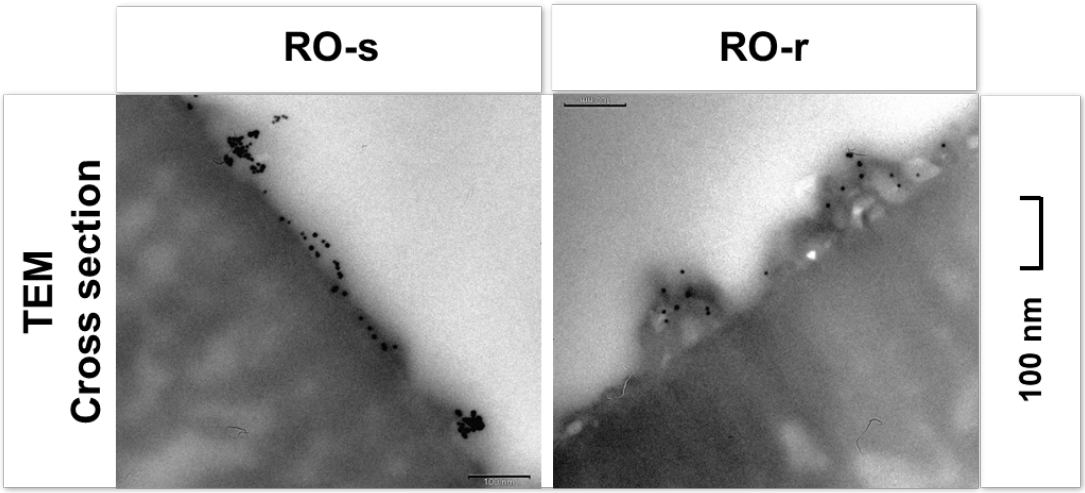

Figure 5. TEM images (cross-sectional view) of gold nanoparticles deposited on RO-s and RO-r.

To further illustrate the impact of surface roughness structures on water transport pathways, we conducted tracer filtration tests using gold nanoparticles (AuNPs) of 5 nm in diameter. Due to the very small size of these AuNPs, they tend to follow the streamlines and preferentially deposit at sites with high localized water flux.[31, 45, 57, 58] In the current study, the AuNPs (represented by the darker particles in the images) were deposited like patches on the relatively smooth surface of RO-s (Figure 5 and Figure S3), which is consistent with the more uneven flux distribution and presence of localized hot spots of high flux as a result of the 'funnel effect' in this membrane (Figure 1a). In contrast, less AuNPs were observed on the RO-r surface, which could possibly be attributed to the decreased localized average flux over the RO-r surface caused by the increased effective membrane filtration area, leading to reduced hydrodynamic drag force on AuNPs towards RO-r surface.[8, 9, 59] In the current study, the AuNPs on the RO-r membrane were mainly distributed on the 'ridges' of the roughness features (Figure 5 and Figure S3), which could be possibly explained by

shortened water transport pathway and thus less hydraulic resistance through the polyamide film above the nanovoid-containing ‘ridges’ (Figure 1b).

Fouling propensity of RO-s and RO-r.

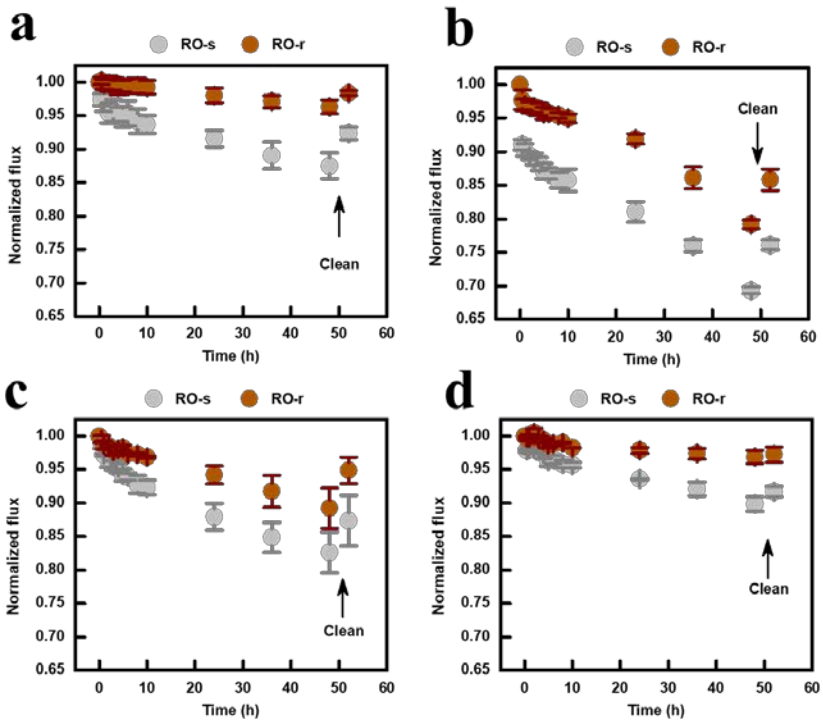

Figure 6. Fouling propensity of RO-s and RO-r using HA as a model foulant in feed solution (100 ppm HA in 2000 ppm NaCl): (a) at initial flux of 20 L m^{-2} h^{-1}, pH at ~6.5, without Ca^{2+}; (b) at initial flux of 20 L m^{-2} h^{-1}, pH at ~4.0, without Ca^{2+}; (c) at initial flux of 20 L m^{-2} h^{-1}, pH at ~6.5, with 0.1 mM Ca^{2+}; (d) at initial flux of 15 L m^{-2} h^{-1}, pH at ~6.5, with 0.1 mM Ca^{2+}. To achieve an identical initial flux of 20 L m^{-2} h^{-1}, the applied pressure for RO-s and RO-r were about ~25 and ~11 bar, respectively. The pressure values were ~20 and ~8.5 bar, respectively, for the initial flux of 15 L m^{-2} h^{-1}. All fouling tests were performed in at least triplicates.

Figure 6a presents fouling by HA for RO-r and RO-s at an identical initial flux of 20 L m^{-2} h^{-1} without the presence of calcium in the feed solution. RO-s experienced faster flux decline (grey circles in Figure 6a) than that of RO-r (red circles in Figure 6a). This observation can be explained by the 'funnel effect' in RO-s (Figure 1a), leading to more uneven flux distribution and higher fouling propensity. In contrast, RO-r gave a mitigated fouling propensity thanks to the modified water transport pathway (Figure 1b), which is consistent with the AuNPs deposition behavior presented in the section 'Water transport pathway of RO-s and RO-r'. Furthermore, the nanovoid-containing membrane RO-r offers

greater effective filtration area (Table 1), which is beneficial to reduce the average localized flux and thus mitigate fouling due to reduced permeate drag force.[9, 34, 38] In addition, previous studies[34, 38] suggested that a decreased localized flux may mitigate the localized concentration polarization, which may further reduce the fouling tendency. It is worthwhile to note that the observed flux in practice is the macroscale apparent flux (J_v) given by the total flow rate (Q) normalized by the membrane plan area (a), i.e., $J_v = Q/a$. In contrast, the average localized water flux ($\overline{J_v}$) at the microscale is related to the actual effective filtration area (a_{eff}) such that $\overline{J_v} = Q/a_{eff}$ (or $\overline{J_v} = J_v/(a_{eff}/a)$). In the current study, RO-r and RO-s had surface area ratios (a_{eff}/a) of 2.98 and 1.16 (Table 1), respectively. For the observed initial flux of 20 L m^{-2} h^{-1} in Figure 6a, this translates to very different $\overline{J_v}$ values: 6.7 L m^{-2} h^{-1} for RO-r vs. 17.2 L m^{-2} h^{-1} for RO-s. This drastically reduced average localized flux, in addition to the mitigation of 'funnel effect', explains the improved anti-fouling performance of the nanovoid-containing membrane RO-r with a rougher surface (Figure 1). To resolve these two effects, we further tested the smooth membrane at a lower apparent initial flux of 7.8 L m^{-2} h^{-1} (marked as RO-s* in Figure 7). In this case, since both RO-r and RO-s* had an identical $\overline{J_v}$ of 6.7 L m^{-2} h^{-1}, the more stable flux for RO-r is attributed to the improved flux distribution due to the mitigation of 'funnel effect'. At the same time, the difference between RO-s* and RO-s reflects the role of average localized flux. Our results reveal that both the decreased average localized flux and the improved flux distribution contribute to better antifouling performance of RO-r, although the former effect appears to be more important.

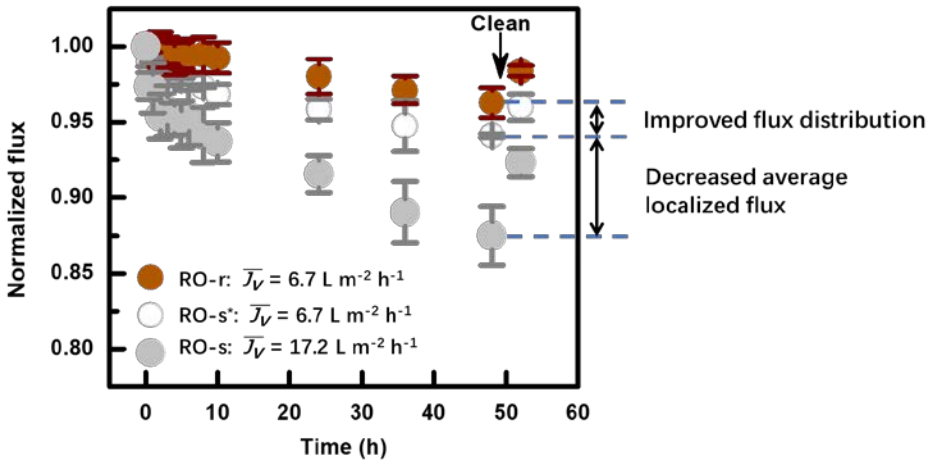

Figure 7. Revolving the role of improved flux distribution and decreased average localized flux on HA fouling (100 ppm HA in 2000 ppm NaCl, pH at ~6.5). RO-s and RO-r had the same apparent flux of 20 L m^{-2} h^{-1}, corresponding to different average localized fluxes ($\overline{J_v}$ = 17.2 L m^{-2} h^{-1} for RO-s and 6.7 L m^{-2} h^{-1} for RO-r). At the same time, RO-s*, with a lower apparent flux of 7.8 L m^{-2} h^{-1}, had an identical average localized flux to that of RO-r ($\overline{J_v}$ of 6.7 L m^{-2} h^{-1}). All fouling tests were performed in at least triplicates.

Additional fouling tests were performed at pH 4.0 to exclude the effect of ionized carboxyl groups on fouling propensity. Under this test condition, although both the surfaces of RO-s and RO-r were weakly charged (Figure 4c) with comparable ionized carboxyl group density (Figure 4d), RO-r still showed better anti-fouling performance than RO-s (Figure 6b). Furthermore, fouling tests were also conducted with 0.1 mM Ca^{2+} included in feedwater.[9, 60, 61] With the same initial flux of 20 L m^{-2} h^{-1}, the presence of 0.1 mM calcium increased the rate of flux decline (Figure 6c), which is attributed to the binding of calcium to HA that causes charge neutralization and bridging effects.[9, 60, 61] Nevertheless, RO-s still had higher fouling propensity than RO-r, which echoes the critical impact of 'funnel effect' on membrane fouling.[31] In addition, since initial flux is also an important parameter affecting membrane fouling,[9, 61, 62] we further performed fouling tests under a lower initial flux of 15 L m^{-2} h^{-1}. RO-r gave a much better antifouling performance at this lower flux (Figure 6d) than that at 20 L m^{-2} h^{-1} (Figure 6c), which can be explained by the decreased

316 hydrodynamic drag force on foulants towards RO-r surface.[8, 9, 59] In contrast, RO-s
317 presented less obvious improvement on its fouling propensity at the lower initial flux. This
318 can be due to the intrinsically non-uniform flux distribution for RO-s, leading to hot spots
319 of high water flux and thus fast foulant deposition. As a result, the hot spots (i.e., the main
320 water transport pathways in RO-s) could be easily blocked by the foulants at even a lower
321 initial flux.

322 In addition, RO-s and RO-r fouled under various test conditions (Figure 8) were cleaned
323 with DI water to access the fouling reversibility. For all cases (T1-T4), RO-r experienced
324 less irreversible fouling than RO-s, which can be attributed to its lower average localized
325 flux with more uniform flux distribution. A lower flux reduces permeation drag, which
326 tends to form a less compact foulant layer[34, 61, 63-66] that could be easier to clean. Consistent
327 with this explanation, reducing the apparent initial flux under otherwise identical testing
328 conditions (Figure 8 T4 vs. T3) also resulted in less irreversible flux loss. For a given
329 membrane, reducing pH (T2 vs. T1) and increasing calcium concentration (T3 vs. T1)
330 resulted in more irreversible flux reduction. These conditions promote the formation of
331 denser foulant layers with stronger foulant-foulant adhesion.[18, 60, 67, 68]

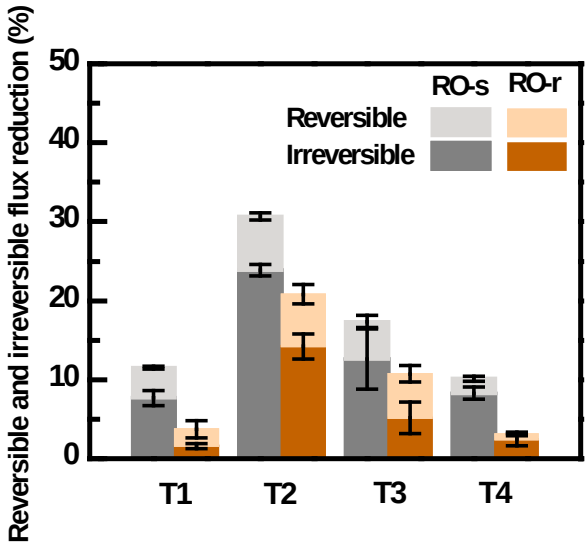

Figure 8. Reversible and irreversible flux reductions for RO-s and RO-r using HA as a model foulant in a feed solution containing 100 ppm HA and 2000 ppm NaCl. Other testing conditions: (T1) initial flux of 20 L m^{-2} h^{-1}, pH ~6.5, without Ca^{2+}; (T2) initial flux of 20 L m^{-2} h^{-1}, pH ~4.0, without Ca^{2+}; (T3) initial flux of 20 L m^{-2} h^{-1}, pH ~6.5, with 0.1 mM Ca^{2+}; (T4) initial flux of 15 L m^{-2} h^{-1}, pH ~6.5, with 0.1 mM Ca^{2+}. All tests were performed in at least triplicates. The corresponding flux recovery data are presented in Supporting Information S5.

IMPLICATIONS

The current study compared the fouling propensity of a smooth (RO-s) and a nanovoid-containing rough (RO-r) polyamide membrane. RO-s suffered more severe fouling by HA than RO-r. Additional AuNPs tracer tests also revealed a less uniform flux distribution over RO-s. These results confirm our hypothesis that nanovoids contained in a rougher membrane can effectively regulate the water transport pathway to result in an improved anti-fouling performance. Our observations seem to contradict with the commonly accepted wisdom that rougher membranes have higher fouling propensity.[15, 17, 18] In reality, membrane fouling can be highly complicated. For example, when a membrane experienced severe fouling conditions, its surface could be fully covered by the foulants. The dominance of foulant—deposited-foulant interaction over foulant—membrane interaction under this scenario may result in a membrane-independent fouling behavior.[62, 68] This mechanism could potentially help to explain why Jiang et al. observed insignificant differences of fouling behaviors between smooth and rough membranes.[69] We also noted that Jiang et al.'s study used different substrates for the smooth and rough membranes,[69] which may complicate the comparison.[70]

Although the current study primarily focused on HA fouling, a similar trend (i.e., RO-r had less fouling propensity) was also observed for another model foulant–bovine serum albumin (Figure S7). However, other effects such as the size of foulant relative to the roughness structure[18] and roughness-enhanced mass transfer[21-24] can also impact membrane fouling. For colloidal fouling, some colloids are of similar size to those of the roughness valleys such that they are more likely to be trapped, which may promote more severe fouling.[18] Several studies have also reported more severe biofouling for rougher

membranes.[18, 71-73] Future studies are needed to further investigate the various competing mechanisms in order to gain a more holistic understanding on the role of roughness on various types of fouling (organic fouling, colloidal fouling, biofouling, and scaling).

At present, membrane surface roughness is typically characterized by AFM in term of common roughness parameters such as average roughness R_A, root-mean-square roughness R_{RMS}, and maximum roughness R_{MAX}. However, these roughness parameters are insufficient to completely describe a roughness structure.[26, 74] For example, roughness structures that have identical roughness values (e.g., R_{MAX} is given by half of the peak-to-valley height) can have different geometrical properties (e.g., aspect ratio), which may lead to very different mass transfer and fouling behaviors. Therefore, researchers need to be explicitly aware of such intrinsic limitations of roughness parameters obtained from AFM. At the same time, more comprehensive characterization of roughness structures and better understanding of specific effect of roughness structures (including geometries) on mass transfer and fouling are needed in future studies.

ASSOCIATED CONTENT

Supporting Information

The Supporting Information is available free of charge at.

S1, Dissolving PSf substrate for observing the backside of polyamide layer; S2, Characterization of ionized carboxyl group density in polyamide layer; S3, Characterizations of polyamide membranes; S4, The effects of applied pressure and cross-flow on fouling propensity; S5, Flux recovery efficiency of RO-s and RO-r; S6, Fouling propensity of RO-s and RO-r using BSA

AUTHOR INFORMATION

Corresponding Authors

Lu Elfa Peng − *Department of Civil Engineering, The University of Hong Kong, Pokfulam, Hong Kong SAR 999077, P. R., China;* Phone: +852 53964327; Email: elfapeng@connect.hku.hk

Chuyang Y. Tang − *Department of Civil Engineering, The University of Hong Kong, Pokfulam, Hong Kong SAR 999077, P. R., China;* orcid.org/0000-0002-7932-6462; Phone: +852 28591976; Email: tangc@hku.hk

Authors

Qimao Gan − *Department of Civil Engineering, The University of Hong Kong, Pokfulam, Hong Kong SAR 999077, P. R., China;*

Chenyue Wu − *Department of Civil Engineering, The University of Hong Kong, Pokfulam, Hong Kong SAR 999077, P. R., China;*

Li Long − *Department of Civil Engineering, The University of Hong Kong, Pokfulam, Hong Kong SAR 999077, P. R., China;*

Zhe Yang − *Department of Civil Engineering, The University of Hong Kong, Pokfulam, Hong Kong SAR 999077, P. R., China;* orcid.org/0000-0003-0753-3902

Hao Guo − *Department of Civil Engineering, The University of Hong Kong, Pokfulam, Hong Kong SAR 999077, P. R., China;*

Notes

The authors declare no competing financial interest.

ACKNOWLEDGMENTS

The work was fully supported by a grant from the Research Grants Council of the Hong Kong Special Administration Region, China (SRFS2021-7S04). Lu Elfa Peng is supported by an RGC Postdoctoral Fellowship from the Research Grants Council of the Hong Kong Special Administration Region, China (PDFS2223-7S02). We appreciate the Electron Microscopic Unit (EMU) of the University of Hong Kong for SEM and TEM sample preparation and analysis.

REFERENCES

1. Lu, X.; Elimelech, M., Fabrication of desalination membranes by interfacial polymerization: history, current efforts, and future directions. Chem. Soc. Rev. 2021, 50, (11), 6290-6307.

2. Elimelech, M.; Phillip, W. A., The future of seawater desalination: energy, technology, and the environment. Science 2011, 333, (6043), 712-7.

3. Tang, C. Y.; Yang, Z.; Guo, H.; Wen, J. J.; Nghiem, L. D.; Cornelissen, E., Potable Water Reuse through Advanced Membrane Technology. Environ. Sci. Technol. 2018, 52, (18), 10215-10223.

4. Qasim, M.; Badrelzaman, M.; Darwish, N. N.; Darwish, N. A.; Hilal, N., Reverse osmosis desalination: A state-of-the-art review. Desalination 2019, 459, 59-104.

5. Yang, Z.; Guo, H.; Tang, C. Y. Y., The upper bound of thin-film composite (TFC) polyamide membranes for desalination. J. Membr. Sci. 2019, 590, 117297.

6. Guo, H.; Dai, R.; Xie, M.; Peng, L. E.; Yao, Z.; Yang, Z.; Nghiem, L. D.; Snyder, S. A.; Wang, Z.; Tang, C. Y., Tweak in Puzzle: Tailoring Membrane Chemistry and Structure toward Targeted Removal of Organic Micropollutants for Water Reuse. Environ. Sci. Technol. Lett. 2022, 9, (4), 247-257.

7. Kang, G. D.; Cao, Y. M., Development of antifouling reverse osmosis membranes for water treatment: A review. Water Res. 2012, 46, (3), 584-600.

8. Tang, C. Y.; Fu, Q. S.; Criddle, C. S.; Leckie, J. O., Effect of flux (transmembrane pressure) and membrane properties on fouling and rejection of reverse osmosis and nanofiltration membranes treating perfluorooctane sulfonate containing wastewater. Environ. Sci. Technol. 2007, 41, (6), 2008-14.

9. Tang, C. Y.; Kwon, Y.-N.; Leckie, J. O., Fouling of reverse osmosis and nanofiltration membranes by humic acid—Effects of solution composition and hydrodynamic conditions. J. Membr. Sci. 2007, 290, (1-2), 86-94.

10. Freger, V.; Ramon, G. Z., Polyamide desalination membranes: Formation, structure, and properties. Prog. Polym. Sci. 2021, 122, 101451.

11. Rana, D.; Matsuura, T., Surface modifications for antifouling membranes. Chem. Rev. 2010, 110, (4), 2448-71.

12. Mo, H.; Tay, K. G.; Ng, H. Y., Fouling of reverse osmosis membrane by protein (BSA): Effects of pH, calcium, magnesium, ionic strength and temperature. J. Membr. Sci. 2008, 315, (1-2), 28-35.

13. Li, Q.; Xu, Z.; Pinnau, I., Fouling of reverse osmosis membranes by biopolymers in wastewater secondary effluent: Role of membrane surface properties and initial permeate flux. J. Membr. Sci. 2007, 290, (1-2), 173-181.

14. Guo, H.; Li, X.; Yang, W.; Yao, Z.; Mei, Y.; Peng, L. E.; Yang, Z.; Shao, S.; Tang, C. Y., Nanofiltration for drinking water treatment: a review. Front Chem Sci Eng 2022, 16, (5), 681-698.

15. Vrijenhoek, E. M.; Hong, S.; Elimelech, M., Influence of membrane surface properties on initial rate of colloidal fouling of reverse osmosis and nanofiltration membranes. J. Membr. Sci. 2001, 188, (1), 115-128.

16. Hoek, E. M. V.; Bhattacharjee, S.; Elimelech, M., Effect of membrane surface roughness on colloid-membrane DLVO interactions. Langmuir 2003, 19, (11), 4836-4847.

17. Elimelech, M.; Zhu, X. H.; Childress, A. E.; Hong, S. K., Role of membrane surface morphology in colloidal fouling of cellulose acetate and composite aromatic polyamide reverse osmosis membranes. J. Membr. Sci. 1997, 127, (1), 101-109.

18. Shang, C.; Pranantyo, D.; Zhang, S., Understanding the Roughness-Fouling Relationship in Reverse Osmosis: Mechanism and Implications. Environ. Sci. Technol. 2020, 54, (8), 5288-5296.

19. Chowdhury, M. R.; Steffes, J.; Huey, B. D.; McCutcheon, J. R., 3D printed polyamide membranes for desalination. Science 2018, 361, (6403), 682-685.

20. Yin, Z.; Yang, C.; Long, C.; Li, A., Influence of surface properties of RO membrane on membrane fouling for treating textile secondary effluent. Environ Sci Pollut Res Int 2017, 24, (19), 16253-16262.

21. Choi, W.; Lee, C.; Lee, D.; Won, Y. J.; Lee, G. W.; Shin, M. G.; Chun, B.; Kim, T.-S.; Park, H.-D.; Jung, H. W.; Lee, J. S.; Lee, J.-H., Sharkskin-mimetic desalination membranes with ultralow biofouling. Journal of Materials Chemistry A 2018, 6, (45), 23034-23045.

22. Maruf, S. H.; Greenberg, A. R.; Pellegrino, J.; Ding, Y., Fabrication and characterization of a surface-patterned thin film composite membrane. J. Membr. Sci. 2014, 452, 11-19.

23. Lee, Y. K.; Won, Y.-J.; Yoo, J. H.; Ahn, K. H.; Lee, C.-H., Flow analysis and fouling on the patterned membrane surface. J. Membr. Sci. 2013, 427, 320-325.

24. Shang, W. T.; Sun, F. Y.; Jia, W.; Guo, J. X.; Yin, S. M.; Wong, P. W.; An, A. K., High-performance nanofiltration membrane structured with enhanced stripe nano-morphology. J. Membr. Sci. 2020, 600, 117852.

25. Istirokhatun, T.; Lin, Y.; Shen, Q.; Guan, K.; Wang, S.; Matsuyama, H., Ag-based nanocapsule-regulated interfacial polymerization Enables synchronous nanostructure towards high-performance nanofiltration membrane for sustainable water remediation. J. Membr. Sci. 2022, 645, 120196.

26. Ma, X.; Yang, Z.; Yao, Z.; Guo, H.; Xu, Z.; Tang, C. Y., Tuning roughness features of thin film composite polyamide membranes for simultaneously enhanced permeability, selectivity and anti-fouling performance. J. Colloid Interface Sci. 2019, 540, 382-388.

27. Gan, Q.; Peng, L. E.; Guo, H.; Yang, Z.; Tang, C. Y., Cosolvent-Assisted Interfacial Polymerization toward Regulating the Morphology and Performance of Polyamide Reverse Osmosis Membranes: Increased m-Phenylenediamine Solubility or Enhanced Interfacial Vaporization? Environ. Sci. Technol. 2022, 56, (14), 10308-10316.

28. Lonsdale, H. K.; Riley, R. L.; Lyons, C. R., Transport in Composite Reverse Osmosis Membranes - Inde. Abstracts of Papers of the American Chemical Society 1971, 101-122.

29. Wijmans, J. G.; Hao, P., Influence of the porous support on diffusion in composite membranes. J. Membr. Sci. 2015, 494, 78-85.

30. Peng, L. E.; Yang, Z.; Long, L.; Zhou, S.; Guo, H.; Tang, C. Y., A critical review on porous substrates of TFC polyamide membranes: Mechanisms, membrane performances, and future perspectives. J. Membr. Sci. 2022, 641, 119871.

31. Long, L.; Wu, C.; Yang, Z.; Tang, C. Y., Carbon Nanotube Interlayer Enhances Water Permeance and Antifouling Performance of Nanofiltration Membranes: Mechanisms and Experimental Evidence. Environ. Sci. Technol. 2022, 56, (4), 2656-2664.

32. Yang, Z.; Wang, F.; Guo, H.; Peng, L. E.; Ma, X. H.; Song, X. X.; Wang, Z.; Tang, C. Y., Mechanistic Insights into the Role of Polydopamine Interlayer toward Improved Separation Performance of Polyamide Nanofiltration Membranes. Environ. Sci. Technol. 2020, 54, (18), 11611-11621.

33. Kattula, M.; Ponnuru, K.; Zhu, L.; Jia, W.; Lin, H.; Furlani, E. P., Designing ultrathin film composite membranes: the impact of a gutter layer. Sci Rep 2015, 5, 15016.

34. Ramon, G. Z.; Wong, M. C. Y.; Hoek, E. M. V., Transport through composite membrane, part 1: Is there an optimal support membrane? J. Membr. Sci. 2012, 415-416, 298-305.

35. Li, X. S.; Li, Q.; Fang, W. X.; Wang, R.; Krantz, W. B., Effects of the support on the characteristics and permselectivity of thin film composite membranes. J. Membr. Sci. 2019, 580, 12-23.

36. Shao, S.; Zeng, F.; Long, L.; Zhu, X.; Peng, L. E.; Wang, F.; Yang, Z.; Tang, C. Y., Nanofiltration Membranes with Crumpled Polyamide Films: A Critical Review on Mechanisms, Performances, and Environmental Applications. Environ. Sci. Technol. 2022, 56, (18), 12811-12827.

37. Wang, F.; Yang, Z.; Tang, C. Y., Modeling Water Transport in Interlayered Thin-Film Nanocomposite Membranes: Gutter Effect vs Funnel Effect. Acs Es&T Engineering 2022, 2, (11), 2023-2033.

38. Ramon, G. Z.; Hoek, E. M. V., Transport through composite membranes, part 2: Impacts of roughness on permeability and fouling. J. Membr. Sci. 2013, 425-426, 141-148.

39. Wong, M. C. Y.; Lin, L.; Coronell, O.; Hoek, E. M. V.; Ramon, G. Z., Impact of liquid-filled voids within the active layer on transport through thin-film composite membranes. J. Membr. Sci. 2016, 500, 124-135.

40. Ma, X.-H.; Yao, Z.-K.; Yang, Z.; Guo, H.; Xu, Z.-L.; Tang, C. Y.; Elimelech, M., Nanofoaming of Polyamide Desalination Membranes To Tune Permeability and Selectivity. Environ. Sci. Technol. Lett. 2018, 5, (2), 123-130.

41. Song, X.; Gan, B.; Qi, S.; Guo, H.; Tang, C. Y.; Zhou, Y.; Gao, C., Intrinsic Nanoscale Structure of Thin Film Composite Polyamide Membranes: Connectivity, Defects, and Structure-Property Correlation. Environ. Sci. Technol. 2020, 54, (6), 3559-3569.

42. Song, X.; Gan, B.; Yang, Z.; Tang, C. Y.; Gao, C., Confined nanobubbles shape the surface roughness structures of thin film composite polyamide desalination membranes. J. Membr. Sci. 2019, 582, 342-349.

43. Peng, L. E.; Jiang, Y.; Wen, L.; Guo, H.; Yang, Z.; Tang, C. Y., Does interfacial vaporization of organic solvent affect the structure and separation properties of polyamide RO membranes? J. Membr. Sci. 2021, 625, 119173.

44. Lin, L.; Lopez, R.; Ramon, G. Z.; Coronell, O., Investigating the void structure of the polyamide active layers of thin-film composite membranes. J. Membr. Sci. 2016, 497, 365-376.

45. Pacheco, F.; Sougrat, R.; Reinhard, M.; Leckie, J. O.; Pinnau, I., 3D visualization of the internal nanostructure of polyamide thin films in RO membranes. J. Membr. Sci. 2016, 501, 33-44.

46. An, H.; Smith, J. W.; Ji, B.; Cotty, S.; Zhou, S.; Yao, L.; Kalutantirige, F. C.; Chen, W.; Ou, Z.; Su, X.; Feng, J.; Chen, Q., Mechanism and performance relevance of nanomorphogenesis in polyamide films revealed by quantitative 3D imaging and machine learning. Sci Adv 2022, 8, (8), eabk1888.

47. Culp, T. E.; Khara, B.; Brickey, K. P.; Geitner, M.; Zimudzi, T. J.; Wilbur, J. D.; Jons, S. D.; Roy, A.; Paul, M.; Ganapathysubramanian, B.; Zydney, A. L.; Kumar, M.; Gomez, E. D., Nanoscale control of internal inhomogeneity enhances water transport in desalination membranes. Science 2021, 371, (6524), 72-75.

48. Kwak, S. Y.; Jung, S. G.; Kim, S. H., Structure-motion-performance relationship of flux-enhanced reverse osmosis (RO) membranes composed of aromatic polyamide thin films. Environ. Sci. Technol. 2001, 35, (21), 4334-4340.

49. Kim, S. H.; Kwak, S. Y.; Suzuki, T., Positron annihilation spectroscopic evidence to demonstrate the flux-enhancement mechanism in morphology-controlled thin-film-composite (TFC) membrane. Environ. Sci. Technol. 2005, 39, (6), 1764-1770.

50. Hirose, M.; Ito, H.; Kamiyama, Y., Effect of skin layer surface structures on the flux behaviour of RO membranes. J. Membr. Sci. 1996, 121, (2), 209-215.

51. Coronell, O.; Marinas, B. J.; Zhang, X. J.; Cahill, D. G., Quantification of functional groups and modeling of their ionization behavior in the active layer of FT30 reverse osmosis membrane. Environ. Sci. Technol. 2008, 42, (14), 5260-5266.

52. Chen, D.; Werber, J. R.; Zhao, X.; Elimelech, M., A facile method to quantify the carboxyl group areal density in the active layer of polyamide thin-film composite membranes. J. Membr. Sci. 2017, 534, 100-108.

53. Peng, L. E.; Yao, Z.; Liu, X.; Deng, B.; Guo, H.; Tang, C. Y., Tailoring Polyamide Rejection Layer with Aqueous Carbonate Chemistry for Enhanced Membrane Separation: Mechanistic Insights, Chemistry-Structure-Property Relationship, and Environmental Implications. Environ. Sci. Technol. 2019, 53, (16), 9764-9770.

54. Park, S.-J.; Lee, M.-S.; Choi, W.; Lee, J.-H., Biocidal surfactant-assisted fabrication of thin film composite membranes with excellent and durable anti-biofouling performance. Chem. Eng. J. 2022, 431, 134114.

55. Peng, L. E.; Yao, Z.; Yang, Z.; Guo, H.; Tang, C. Y., Dissecting the Role of Substrate on the Morphology and Separation Properties of Thin Film Composite Polyamide Membranes: Seeing Is Believing. Environ. Sci. Technol. 2020, 54, (11), 6978-6986.

56. Peng, L. E.; Gan, Q. M.; Yang, Z.; Wang, L.; Sun, P. F.; Guo, H.; Park, H. D.; Tang, C. Y., Deciphering the Role of Amine Concentration on Polyamide Formation toward Enhanced RO Performance. Acs ES&T Engineering 2022, 2, (5), 903-912.

57. Li, Y.; Kłosowski, M. M.; McGilvery, C. M.; Porter, A. E.; Livingston, A. G.; Cabral, J. T., Probing flow activity in polyamide layer of reverse osmosis membrane with nanoparticle tracers. J. Membr. Sci. 2017, 534, 9-17.

58. Pacheco, F. A.; Pinnau, I.; Reinhard, M.; Leckie, J. O., Characterization of isolated polyamide thin films of RO and NF membranes using novel TEM techniques. J. Membr. Sci. 2010, 358, (1-2), 51-59.

59. Boo, C.; Elimelech, M.; Hong, S., Fouling control in a forward osmosis process integrating seawater desalination and wastewater reclamation. J. Membr. Sci. 2013, 444, 148-156.

60. Listiarini, K.; Sun, D. D.; Leckie, J. O., Organic fouling of nanofiltration membranes: Evaluating the effects of humic acid, calcium, alum coagulant and their combinations on the specific cake resistance. J. Membr. Sci. 2009, 332, (1-2), 56-62.

61. Tang, C. Y.; Chong, T. H.; Fane, A. G., Colloidal interactions and fouling of NF and RO membranes: a review. Adv. Colloid Interface Sci. 2011, 164, (1-2), 126-43.

62. Tang, C. Y.; Leckie, J. O., Membrane independent limiting flux for RO and NF membranes fouled by humic acid. Environ. Sci. Technol. 2007, 41, (13), 4767-73.

63. Wang, S.; Guillen, G.; Hoek, E. M., Direct observation of microbial adhesion to membranes. Environ. Sci. Technol. 2005, 39, (17), 6461-9.

64. Ramon, G. Z.; Huppert, H. E.; Lister, J. R.; Stone, H. A., On the hydrodynamic interaction between a particle and a permeable surface. Phys. Fluids 2013, 25, (7), 073103.

65. Choi, H.; Zhang, K.; Dionysiou, D.; Oerther, D.; Sorial, G., Effect of permeate flux and tangential flow on membrane fouling for wastewater treatment. Sep. Purif. Technol. 2005, 45, (1), 68-78.

66. Chen, V.; Fane, A. G.; Madaeni, S.; Wenten, I. G., Particle deposition during membrane filtration of colloids: Transition between concentration polarization and cake formation. J. Membr. Sci. 1997, 125, (1), 109-122.

67. Tang, C. Y. Y.; Kwon, Y. N.; Leckie, J. O., Characterization of humic acid fouled reverse osmosis and nanofiltration membranes by transmission electron microscopy and streaming potential measurements. Environ. Sci. Technol. 2007, 41, (3), 942-949.

583 68. Tang, C. Y.; Kwon, Y.-N.; Leckie, J. O., The role of foulant–foulant electrostatic interaction on
584 limiting flux for RO and NF membranes during humic acid fouling—Theoretical basis, experimental evidence,
585 and AFM interaction force measurement. J. Membr. Sci. 2009, 326, (2), 526-532.

586 69. Jiang, Z.; Karan, S.; Livingston, A. G., Membrane Fouling: Does Microscale Roughness Matter? Ind.
587 Eng. Chem. Res. 2019, 59, (12), 5424-5431.

588 70. Wu, C.; Long, L.; Yang, Z.; Tang, C. Y., Porous substrate affects fouling propensity of thin-film
589 composite nanofiltration membranes. Journal of Membrane Science Letters 2022, 2, (2), 100036.

590 71. Khan, M. M.; Stewart, P. S.; Moll, D. J.; Mickols, W. E.; Nelson, S. E.; Camper, A. K., Characterization
591 and effect of biofouling on polyamide reverse osmosis and nanofiltration membrane surfaces. Biofouling
592 2011, 27, (2), 173-83.

593 72. Baek, Y.; Yu, J.; Kim, S.-H.; Lee, S.; Yoon, J., Effect of surface properties of reverse osmosis
594 membranes on biofouling occurrence under filtration conditions. J. Membr. Sci. 2011, 382, (1-2), 91-99.

595 73. Pang, C. M.; Hong, P.; Guo, H.; Liu, W. T., Biofilm formation characteristics of bacterial isolates
596 retrieved from a reverse osmosis membrane. Environ. Sci. Technol. 2005, 39, (19), 7541-50.

597 74. Gan, Q.; Peng, E. L.; Yang, Z.; Sun P.; Wang, L.; Guo, H.; Tang, C. Y., Demystifying the role of
598 surfactant in tailoring polyamide morphology for enhanced RO performance: Mechanistic insights and
599 environmental implications. DOI: https://doi.org/10.1021/acs.est.2c08076.